crystals

MDPI

Article

Polydianiline (PDANI) from a Safe Precursor: Dopant-Driven Control of Structure and Electroactivity

Rocco Carcione [1,2,3,*], Emanuela Tamburri [2], Giorgio Scordo [4], Francesca Pescosolido [5], Luca Montaina [5], Elena Palmieri [5], Alessia Cemmi [3] and Silvia Battistoni [6,*]

1 Consiglio Nazionale delle Ricerche, Institute of Materials for Electronics and Magnetism (CNR-IMEM), Parco Area delle Scienze 37A, 43124 Parma, Italy
2 Department of Chemical Sciences, University of Rome "Tor Vergata", Via della Ricerca Scientifica, 00133 Rome, Italy; emanuela.tamburri@uniroma2.eu
3 Nuclear Department (NUC), Agenzia Nazionale per le Nuove Tecnologie, l'Energia e lo Sviluppo Economico Sostenibile (ENEA), Via Anguillarese, Casaccia R.C. 301, 00123 Rome, Italy; alessia.cemmi@enea.it
4 Department of Electronic Engineering, University of Rome "Tor Vergata", Via del Politecnico 1, 00133 Rome, Italy; giorgio.scordo@uniroma2.it
5 Consiglio Nazionale delle Ricerche, Institute for Microelectronics and Microsystems (IMM), Via Fosso Del Cavaliere 100, 00133 Rome, Italy; francesca.pescosolido@artov.imm.cnr.it (F.P.); luca.montaina@artov.imm.cnr.it (L.M.); elena.palmieri@artov.imm.cnr.it (E.P.)
6 Consiglio Nazionale delle Ricerche, Institute of Materials for Electronics and Magnetism (CNR-IMEM) Sezione di Roma, Via della Ricerca Scientifica 1, 00133 Rome, Italy
* Correspondence: rocco.carcione@enea.it (R.C.); silvia.battistoni@imem.cnr.it (S.B.)

Abstract

This work focuses on the synthesis and the comprehensive characterization of polydianiline (PDANI) polymer, obtained via oxidative polymerization of dianiline, a low-toxicity and more environmentally friendly starting monomer for polyaniline (PANI) formation. Despite the structural similarity to PANI, PDANI remains underexplored, especially regarding the effect of different synthesis conditions. Here, we investigate how chloride, sulfate, and camphor sulfonate dopants, combined with green solvents such as water and DMSO, modulate the final properties of PDANI in the emeraldine salt configuration. The produced materials were extensively characterized using a multi-technique approach. FTIR, Raman, EPR, and UV-Vis spectroscopies provided insights into chemical structure, molecular order, and polaron population. Electrical conductivity was disclosed via current-voltage (I-V) measurements, while cyclic voltammetry (CV) and coulovoltammetry (QV) were employed to evaluate redox activity and charge reversibility. The resulting PDANI displays structural and functional features comparable to those of PANI synthesized under similar conditions. Notably, the nature of the dopant and acidic medium was found to crucially govern the oxidation level, molecular organization, and electrochemical performance, boosting PDANI as a tunable and sustainable alternative for applications ranging from electronics to energy storage.

Keywords: polydianiline; polyaniline; N-phenyl-p-phenylenediamine; polaron population; electrically conductive powders

Academic Editor: Mingjun Huang

Received: 8 August 2025
Revised: 10 September 2025
Accepted: 14 September 2025
Published: 17 September 2025

Citation: Carcione, R.; Tamburri, E.; Scordo, G.; Pescosolido, F.; Montaina, L.; Palmieri, E.; Cemmi, A.; Battistoni, S. Polydianiline (PDANI) from a Safe Precursor: Dopant-Driven Control of Structure and Electroactivity. *Crystals* **2025**, *15*, 814. https://doi.org/10.3390/cryst15090814

1. Introduction

Since Hideki Shirakawa's revolutionary discovery in the late 1970s, conducting polymers (CPs) have emerged as a fascinating class of materials at the intersection of organic chemistry and electronics [1]. In particular, the CPs' ability to combine electrical conductivity with the mechanical properties typical of polymeric systems has opened up

extensive research avenues in chemical sensing, supercapacitors, and flexible electronic devices [2–13]. Among CPs, polyaniline (PANI) is acknowledged as one of the most prominent and versatile materials thanks to the combination of superb properties, such as intrinsic redox activity, environmental stability, and relatively simple synthesis [2,3,14–20]. In particular, the tunability of PANI's oxidation states (leucoemeraldine, emeraldine, and pernigraniline), combined with its protonation-dependent conductivity, enables it to function as a responsive material in a wide range of applications, including sensing, electrochromics, supercapacitors, batteries, antimicrobial coatings, and bioelectronics [3,13,20–34]. Among these, most research focuses on synthesizing PANI in its emeraldine salt form, representing the polymer's semi-oxidized state. This form exhibits high electrical conductivity, primarily due to the presence of polarons, which are localized charge carriers with spin produced upon protonation of the emeraldine-base form. These polarons are responsible for charge transport along and between polymer chains, making the emeraldine salt phase the most technologically relevant configuration for electronic and electrochemical applications [22–24,26,35,36].

Despite these intriguing performances, the conventional synthesis of PANI from aniline precursors can face significant drawbacks. As reported in the Material Safety Data Sheet (MSDS), aniline monomer is toxic, volatile, and potentially carcinogenic. Such properties make the handling of aniline problematic from an environmental impact point of view, particularly for applications where biocompatibility and sustainability are crucial [37–39]. This has prompted growing interest in both academic and industrial contexts toward the investigation of greener precursors and alternative synthetic routes to produce materials analogous to PANI [38,40–43].

In this evolving landscape, our previous research has made substantial contributions by innovating both the chemistry and the processing strategies of systems based on PANI and PANI-analogous [30,34,35,39,44,45]. In particular, the most recent ones span from electropolymerized PANI coatings for flexible electronics to the development of photo-cross-linkable PANI composites compatible with 3D printing technologies. The approaches proposed allow for the fabrication of electroactive hydrogels and wearable or implantable soft devices, pushing the boundaries of conducting polymers into the domains of biosensing, smart prosthetics, and electroceuticals. In this context, a particularly notable advancement is given by integrating PANI-based systems within 3D-printable matrices, such as PEGDA-based hydrogels, enabling structural control at the microscale while maintaining electrical functionality [30,34,39]. These hybrid materials, developed through both in situ oxidative polymerization and physical blending, exhibit promising mechanical compliance and electronic activity for soft electronics and stimuli-responsive systems. Nevertheless, despite the growing interest in functional PANI-based composites, a significant gap still exists in the understanding of the intrinsic properties of PANI analogs synthesized from alternative, safer precursors. Therefore, a deep investigation is crucial for a knowledge of the relationships between structural and functional properties of these systems, which would allow us to expand the toolbox of green, tunable materials for use in next-generation electronic and energy devices beyond conventional aniline-derived polymers.

In the scenario of the precursors alternative to aniline, N-phenyl-p-phenylenediamine, also known as dianiline (DANI), a dimeric species of aniline, has an edge for solubility in polar solvents, improved chemical stability, and lower toxicity [38,40–43]. For instance, Galloni et al. [46] have recently demonstrated a green catalytic method for the synthesis of highly porous polyaniline, enabling precise morphology control while reducing environmental impact. These advancements highlight the broader shift toward eco-compatible approaches in the design and fabrication of conductive polymers, aligning with the goals of

sustainability. In particular, the polymerization of DANI allows for producing polydianiline (PDANI), which shares the conjugated backbone structure of PANI and, under similar conditions, exhibits analogous charge-transport behavior [39]. Historically, DANI has been used in copolymerization strategies or as a modifier of aniline-based systems to tailor structural or electronic properties [38,40–43]. More recently, PDANI-based materials have been developed as precursors for N-doped carbon frameworks or embedded in composites for supercapacitor electrodes and metal-ion adsorbents [47]. However, most of these studies focus on PDANI as part of a composite or post-processed system [48–51], rather than characterizing the intrinsic properties of the PDANI phase synthesized solely from DANI.

To overcome this gap, the present study isolates and thoroughly investigates the PDANI polymer obtained by oxidative polymerization of DANI using three distinct dopants, such as chloride (Cl^-), sulfate (SO_4^{2-}), and camphor sulfonate (CS^-). Building upon our recent work on PEGDA–PDANI composites synthesized via in situ polymerization [39], these dopants are chosen for their ionic radius, valence, and chemical reactivity combination. On the same basis [39], the PDANI syntheses were conducted by adapting standard PANI protocols and using green solvents, such as water and DMSO, avoiding the hazards associated with liquid aniline. The produced PDANI systems were characterized through a multi-technique approach. Techniques such as Raman, FTIR, EPR, and UV-Vis spectroscopies were employed to probe structural, chemical composition, and polaron population features, respectively. In addition, I-V measurements allowed for the derivation of the electrical conductivity, while cyclic voltammetry (CV) and coulovoltammetry (QV) analyzed redox properties and charge storage behavior. The coupling of these spectroscopic and electrochemical analyses allowed us to investigate how the dopant identity governs the polaron formation, redox behavior, and functional stability of PDANI.

In particular, this paper is devoted to studying how the dopant nature directly governs the molecular structure, oxidation state, degree of protonation, charge carrier population, and ultimately the electrical and electrochemical performance of the resulting PDANI polymers. Unlike earlier studies centered on doped composites and films, this research provides new insight into the intrinsic properties of isolated PDANI systems, offering a foundation for their future exploitation as a green, tunable alternative to PANI for electronic applications such as batteries, supercapacitors, and biocompatible devices. Additionally, this work contributes to filling a significant gap in the literature by offering a comprehensive study of the pure PDANI phase, enabling more informed design of future functional materials based on DANI-derived systems.

2. Materials and Methods

2.1. Chemicals

N-phenyl-p-phenylenediamine (NPPD or DANI) was purchased by Alfa Aesar (Ward Hill, MA, USA). Ammonium persulphate (APS), dimethyl sulfoxide (DMSO), hydrochloric acid (HCl), sulfuric acid (H_2SO_4), (1S)-(+)-10-camphorsulfonic acid (CSA), and ethanol were purchased from Merck (Darmstadt, Germany) and used as received.

2.2. Synthesis of Pdani Polymers

Three different PDANI polymers were synthesized via chemical oxidative polymerization of the DANI monomer precursor using ammonium persulfate (APS) as the oxidizing agent. The scheme of synthesis is illustrated in Figure 1.

The synthetic route proposed in Figure 1 is analogous to the aniline oxidative polymerization [52]. The process presumably initiates with the oxidation of DANI by APS, generating a radical cation. This radical cation subsequently reacts with another DANI monomer to propagate the polymer chain. Polymerization occurs under acidic conditions,

facilitating both chain growth and protonation, ultimately yielding PDANI in its conductive emeraldine salt (ES) form.

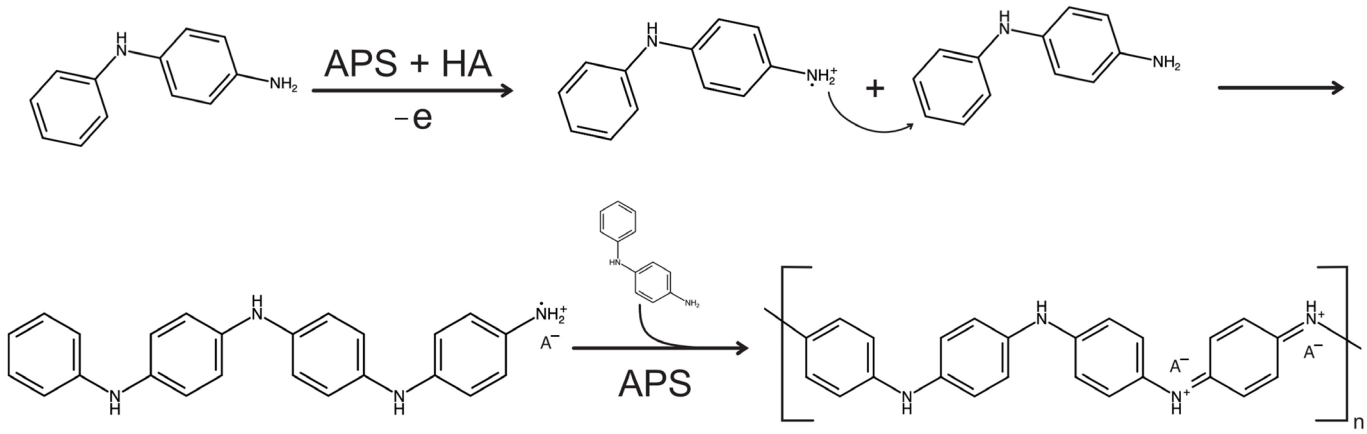

Figure 1. Scheme illustrating the synthesis of PDANI from DANI precursor.

Equimolar amounts of DANI and APS were used. DANI was first dispersed in DMSO, while APS was dissolved in three different acidic aqueous solutions, such as 1 M HCl, 1 M H_2SO_4, and 1 M camphor sulfonic acid (CSA), acting as doping-providing systems. The acidic oxidant solutions were then slowly added dropwise (0.5 mL/min) to the precursor dispersion, maintained at 0–5 °C in an ice bath to control the polymerization rate.

The reactions were allowed to proceed under continuous stirring for 24 h. Upon completion, the resulting dark green PDANI powders were recovered by filtration, followed by successive washing with deionized water and ethanol to remove unreacted species and by-products. The samples were then dried at room temperature in air. For some analysis, the samples were properly pelletized by using a hydraulic press operating at a pressure of 6×10^3 kg cm^{-2} for 1 min. Table 1 provides the sample identifiers and the concentrations of the monomer and dopant solutions used for the syntheses.

Table 1. Sample identifiers and the concentrations of the monomer and dopant solutions used for the syntheses.

Sample Name	Starting Solution		Oxidant Solution		Total Volume	Dopant Agent	Final Solution
	DANI (mmol)	DMSO (mL)	APS (mmol)	Acidic Solution	mL		[DANI] (M)
P-Cl	4	2	4	HCl 1M	80	Cl^-	0.05
P-SO_4	4	2	4	H_2SO_4 1M	80	SO_4^{2-}	0.05
P-CS	4	2	4	CSA 1M	80	CS^-	0.05

In line with other studies [46], The reaction yield was computed according to Equation (1):

$$yield\ (\%) = \frac{mass_{product}}{mass_{precursor} + \frac{mass_{dopant}}{2}} \quad (1)$$

where $mass_{product}$ is the mass of the synthesized PDANI, $mass_{precursor}$ is the mass of dianiline, and $mass_{dopant}$ is the mass the used dopant.

2.3. Characterization Techniques

FTIR spectra were collected in the range 650–2000 cm^{-1} under attenuated total reflectance (ATR) mode by using a ZnSe crystal by means of a Spectrum 100 Perkin-Elmer

FT-IR spectrometer (PerkinElmer Ltd., Beaconsfield, UK). To perform the analysis of each spectrum, the background (i.e., air) was subtracted, and a correction of the baseline was performed. For each sample, three independent spectra were recorded, and the mean values of the analyzed peaks' parameters were used.

Raman spectra were collected in the range between 1000 and 1800 cm^{-1} by means of an Xplora Plus (Horiba Scientific, Kyoto, Japan) instrument, under a laser source at 785 nm, 10% power, 100× magnification, and 3 cm^{-1} spectral resolution with a grating set at 1200T. The Raman spectra were normalized and deconvolved by Lorentz function lines to derive position, amplitude, and integrated intensity for each peak.

Electrical conductivity measurements were performed by recording current-voltage (I-V) characteristics using the four-probe method. The measurement setup employed a Keithley 6221 current source and a Keithley 2700 multimeter (Keithley Instruments, Cleveland, OH, USA), both controlled via a LabVIEW interface. Details are reported in [30]. The IV tests were performed on at least three independent replicas for each typology of PDANI sample.

Electrochemical measurements were carried out in a standard one-compartment three-electrode cell by means of a Palm Sense compact electrochemical workstation. The produced samples were deposited on Pt foils to behave as the working electrode, while a saturated calomel electrode (SCE) and a Pt foil were used as the reference and counter electrode, respectively. Cyclic voltammetry (CV) curves were collected in the $(-0.2 \div +0.8)$ V potential range and at scan rates of 15, 30, 60, 120, and 200 mV/s in 1 M HCl solution. CV measurements were performed over multiple consecutive cycles for each PDANI sample. QV curves were derived by CV using PSTrace software (version 5.9).

EPR spectra were obtained by using an EPR Bruker e-scan spectrometer operating in the X-band, with a frequency of 9.4 GHz, microwave power of 0.14 mW, and magnetic field in the range 3390–3580 G. For this analysis, the samples were positioned in a conventional quartz tube. All the spectra and the EPR data were normalized to the sample mass (approximately 20 mg).

UV-Vis spectra were acquired by a PerkinElmer™ Lambda 950 UV-VIS-IR double-beam spectrophotometer (PerkinElmer Ltd., Beaconsfield, UK), equipped with an integrating sphere, in the range 300–950 nm with a 2 nm step.

3. Results

Figure 2 shows the aspect of the PDANI samples synthesized by using chloride (P-Cl), sulfate (P-SO_4), and camphor sulfonate (P-CS) dopant agents and collected in the form of powders.

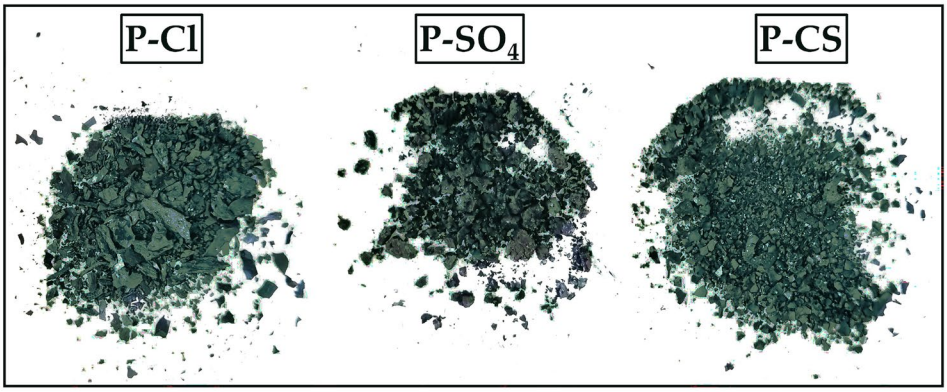

Figure 2. Visual appearance of the PDANI samples synthesized with different dopant agents, i.e., P-Cl (**left**), P-SO_4 (**center**), and P-CS (**right**), and collected in the form of powder.

As shown in Figure 2, after solvent evaporation, all the powders have a granular, compact appearance and look dry and well-consolidated. Each sample exhibits the dark emerald-green color, characteristic of the emeraldine salt (ES) form of polyaniline systems [23,53]. The yield% values were around 95, 90, and 70% for P-Cl, P-SO4, and P-CS samples, respectively. These values are plausibly linked to both the size of the dopant anion and the strength of the acid used during polymerization. In particular, the higher yield obtained with HCl arises from its strong acidity and the small size of Cl^- ions, which favor efficient protonation and doping of PDANI chains. In contrast, bulkier dopants like CS^- and the more complex SO_4^{2-} anions reduce doping efficiency, leading to lower apparent yields.

To evaluate and compare the chemical composition of the PDANI phases, FTIR-ATR spectroscopy analysis was accomplished on the three samples. The FTIR-ATR spectra are reported in Figure 3, along with the main signals' attribution.

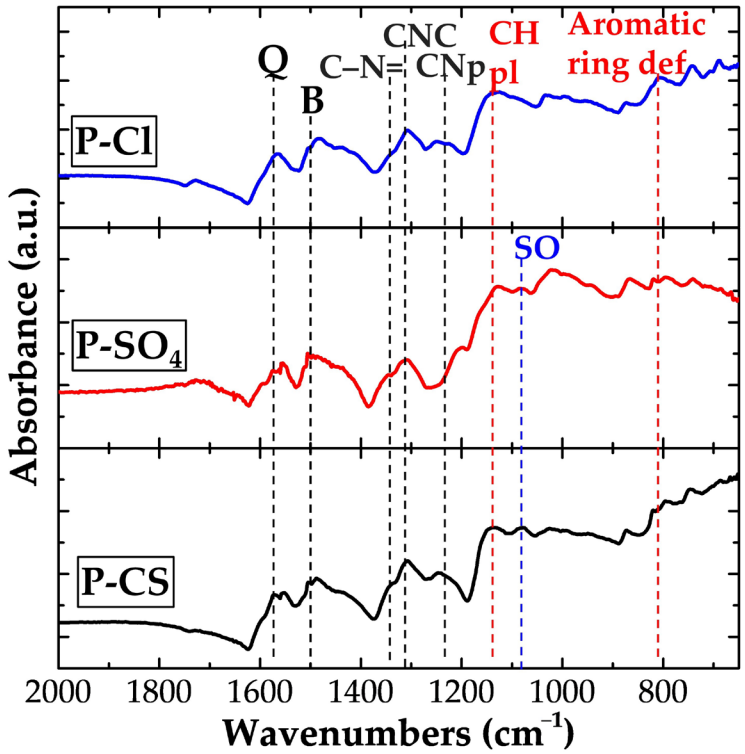

Figure 3. Representative FTIR-ATR spectra of the P-Cl, P-SO_4, and P-CSA PDANI samples, along with the main signals' attribution.

The spectra exhibit the characteristic vibrational features of polyaniline in the ES form [44,54–57]. In particular, the bands located at approximately 1565 cm^{-1} and 1490 cm^{-1} are assigned to the quinoid (Q) and benzenoid (B) ring stretching modes, respectively. The intensity ratio between the peaks of the benzenoid and quinoid form (I_B/I_Q) is around 1 for all samples, indicating a balanced coexistence of the two units within the polymer backbone. This points out the production of the emeraldine semi-oxidized form of PANI, suggesting the formation of delocalized polaronic structures and an efficient protonation level during synthesis. The latter are key factors for ensuring efficient charge transport and high electrical conductivity in doped PANI systems [55,56].

In agreement with these considerations, the presence of a band at ~1375 cm^{-1} is attributed to C–N= stretching between the B and Q units, while bands around 1300 cm^{-1} reflect C–N–C vibrations and π-electron delocalization [55,56]. A strong absorption band at ~1246 cm^{-1} corresponds to the C–N stretching associated with polaron formation. Addi-

tionally, signals in the 1145–1160 cm^{-1} range can be related to in-plane C–H bending modes (C-H pl), indicative of protonation-induced delocalization, and bands below 1000 cm^{-1} can be assigned to out-of-plane C–H deformations and ring vibrations of the substituted aromatic system. Finally, it is interesting to note that the spectra of P-SO_4 and P-CSA samples show a peak at ~1090 cm^{-1}, likely due to the S=O and S–O stretching vibrations of the sulfur-based dopant species [55,58].

Further details on the molecular structure are provided by Raman spectroscopy analysis. Figure 4 shows the Raman spectra recorded for P-Cl, P-SO_4, and P-CS PDANI samples along with the main signals' attribution.

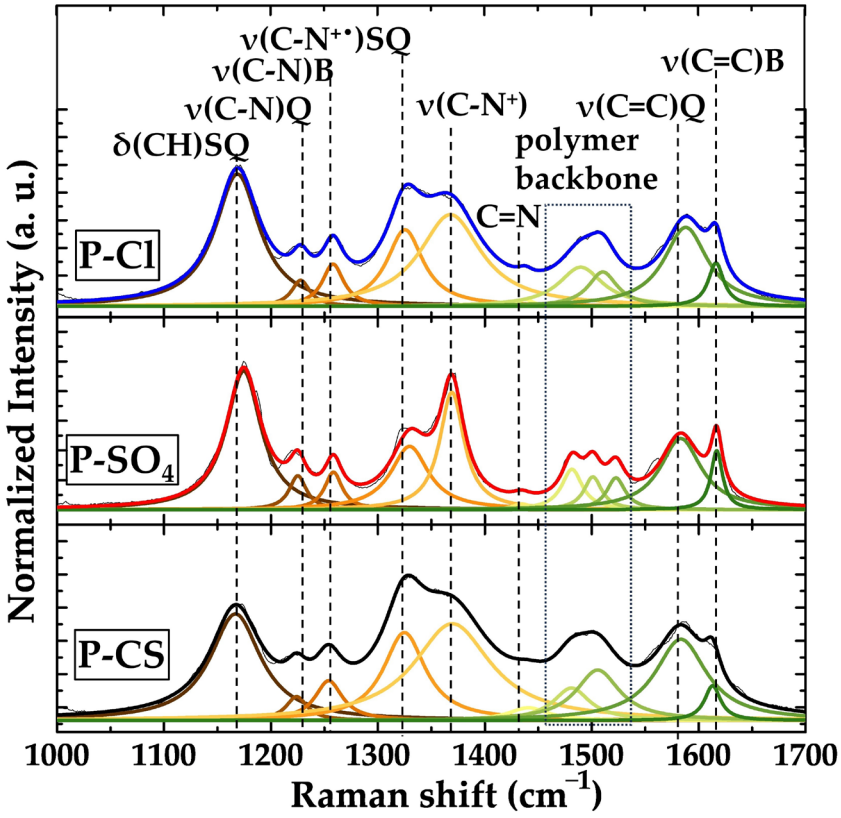

Figure 4. Representative deconvolved Raman spectra of the P-Cl, P-SO_4, and P-CS PDANI samples along with the main signals' attribution.

In line with the FTIR-ATR analysis, the Raman spectra show the typical features of the ES form [22,59,60]. While the spectra are generally similar across the three differently doped polymers, a closer inspection reveals distinctive features in the P-SO_4 sample. In particular, the intensity of the band at ~1380 cm^{-1}, assigned to C–N^+ stretching, is significantly higher in P-SO_4 than in the other samples, suggesting a higher number of oxidized sites [61]. Moreover, the spectral region around 1500 cm^{-1}, typically associated with polymeric backbone vibrations, displays three discernible peaks in P-SO_4, in contrast to the two main contributions observed in P-Cl and P-CS.

Although the ES form is the predominant phase obtained in all synthesized samples, the spectral features of P-SO_4 suggest distinct differences in chain entanglement and molecular ordering compared to the other PDANI samples. This behavior is plausibly linked to the use of sulfuric acid, a well-known strong oxidizing and dehydrating agent. Its dual chemical action likely promotes both the generation of positively charged nitrogen centers (polarons) and the removal or confinement of water molecules within the polymer matrix, thereby influencing interchain interactions [62–64]. These combined effects may result in a tighter, more ordered polymer conformation, structurally differenti-

ating P-SO_4 from samples doped with less aggressive acids and contributing to its unique molecular organization.

In this context, further insights from Raman spectroscopy analysis can be focused on the protonation degree of PDANI backbone. As shown in Figure 4, the signals ascribable to semiquinonoid radical entities in all the three samples' spectra indicate the formation of partially protonated chains, suggesting that the adopted synthetic route effectively promotes polaron formation in the emeraldine phase. In particular, the *protonation percentage* of PDANI systems is evaluated by using Equation (2) [44]:

$$protonation\ percentage\ = \frac{A_{1320}}{A_{1225} + A_{1320}} \cdot 100 \quad (2)$$

where A_{1320} and A_{1225} are the integrated area of the peaks located at 1320 and 1225 cm^{-1}, respectively, attributable to the stretching vibration of the polaronic and benzenoid C-N bond. The calculated values are 82% for P-Cl, 75% for P-SO_4, and 80% for P-CS, all indicating a high degree of protonation and a consequent remarkable doping level for all the produced PDANI systems.

To expand the structural investigation, EPR spectroscopy was employed to evaluate the concentration of polarons, being polymeric chains associated with unpaired electron spins. These species are the main charge carriers in the doped emeraldine form of polyaniline. Therefore, EPR spectroscopy, which directly detects unpaired electrons, provides quantitative insight into the density of charge carriers within the polymer matrix. Figure 5 shows the EPR spectra and the corresponding signal area normalized to sample mass for the three PDANI samples. The EPR signal area values, proportional to the number of radicals present in the samples, were derived by integrating twice the spectra.

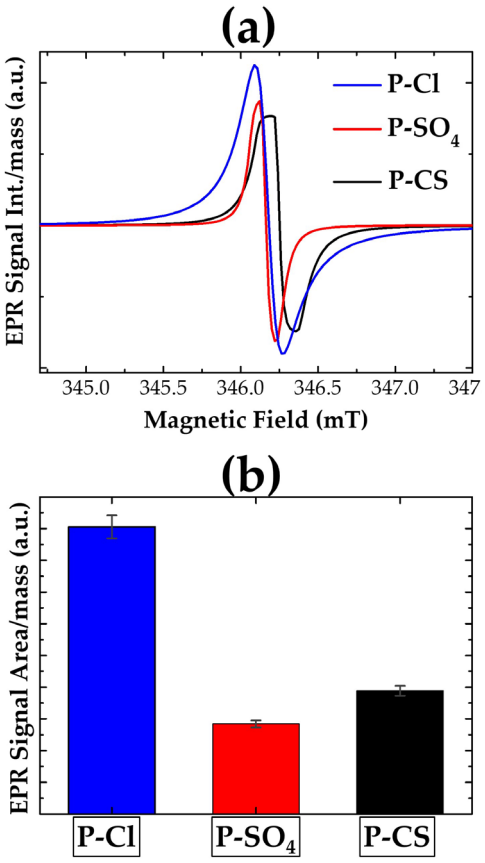

Figure 5. (**a**) EPR spectra and (**b**) corresponding signal area normalized to sample mass for P-Cl, P-SO_4, and P-CS.

Figure 5a reveals differences in both shape and intensity across the samples' spectra. This divergence is consistent with the molecular-level structural differences already highlighted by FTIR and Raman data. In particular, P-Cl and P-CS exhibit broader EPR signals that can be attributed to greater heterogeneity in the local environments of the polarons, possibly due to increased inter-chain interactions, chain entanglement, and charge carriers' mobility within the doped polymer matrix [65–67]. In contrast, P-SO_4 shows a sharper and more defined resonance line, suggesting that the polarons in this sample reside in more uniform, structurally similar molecular environments [67,68]. This could reflect higher chain alignment or molecular order, plausibly induced by the use of sulfuric acid during synthesis, as previously suggested by the Raman spectroscopy analysis.

To better visualize the data, Figure 5b displays the EPR signal areas obtained by double integration of the spectra, reflecting the relative polaron population in each sample. As shown in Figure 5b, P-Cl and P-SO_4 samples respectively show the highest and the lowest polaron concentration, while the P-CS sample, despite its bulkier dopant, exhibits a moderate polaron population level. These results are not unexpected. The use of HCl in the aniline oxidative polymerization is well known to promote high levels of protonation, doping efficiency, and charge carrier density in PANI-based materials [8,62,69,70]. Analogously, the concentration of polarons for P-CS is consistent with the adopted synthesis conditions. Despite the presence of a bulky dopant such as camphor sulfonate, the acidic oxidative polymerization proceeds effectively for P-CS systems, allowing for the incorporation of CS^- ions into the polymer matrix and enabling charge carrier formation.

Conversely, the effect of H_2SO_4 is more complex and has been the subject of extensive discussion in the literature [65–68,71–73]. Several studies report that the doping of polyaniline with sulfate ions produces changes in the polymer electronic structure, tailoring both protonation states and the resonance of the delocalized polaron lattice [71–73]. Additionally, the dehydrating power of sulfuric acid has been shown to influence molecular packing by confining interchain water molecules [72]. This effect promotes hydrogen bonding and lattice strain, contributing to the formation of well-ordered, extended polymer chains. Based on these considerations, the EPR results can be explained by the fact that the P-SO_4 chains are more ordered and entangled with well-positioned water molecules, exhibiting remarkable doping levels. Consequently, polaronic sites are more regularly distributed along the polymeric backbone. However, polaron density in the case of P-SO_4 is lower compared to the other investigated PDANI samples.

In view of these outcomes, the EPR analysis confirms and complements the FTIR and Raman spectroscopies results, reinforcing the idea that dopant identity crucially drives both the quantity and the structural organization of charge carriers in PDANI phase.

Finally, UV-Vis spectra were studied to understand the transition state of the resulting polymers. Figure 6 shows the UV–Vis absorption spectra of pristine PDANI in the 300–950 nm range.

As shown in Figure 6, the PDANI samples UV-Vis spectra exhibit three characteristic absorption bands around 350, 430, and 770 nm, respectively associated with the π–π* transition of benzenoid rings, polaron-to-π* transitions, and localized polarons on protonated imine groups (C=N) and delocalized polarons diagnostic of the emeraldine salt (ES) conductive state of polyaniline derivatives [74–76]. Together with the FTIR, Raman, and EPR spectroscopies results, these spectra confirm that all samples are in the ES form and that the doping process was successfully achieved with each of the tested acids.

A comparison among the samples highlights notable differences in the intensity of the polaronic band at around 770 nm. The UV-Vis spectrum of the P-Cl sample exhibits the most intense polaron absorption, which indicates the highest spin density for this system. On the other hand, the UV-Vis spectra of P-SO_4 and P-CS display weaker polaronic

features relative to the π–π transition. On the basis of Raman and EPR results, this trend can be plausibly related to the dopant nature. In particular, the small chloride ion is easily incorporated into the polymer backbone, ensuring efficient doping, while the bulky camphor sulfonate hinders effective charge delocalization. Sulfate ions introduce a more complex doping environment, leading to the formation of a lower number of delocalized polarons residing in more uniform, structurally similar molecular environments [67,68].

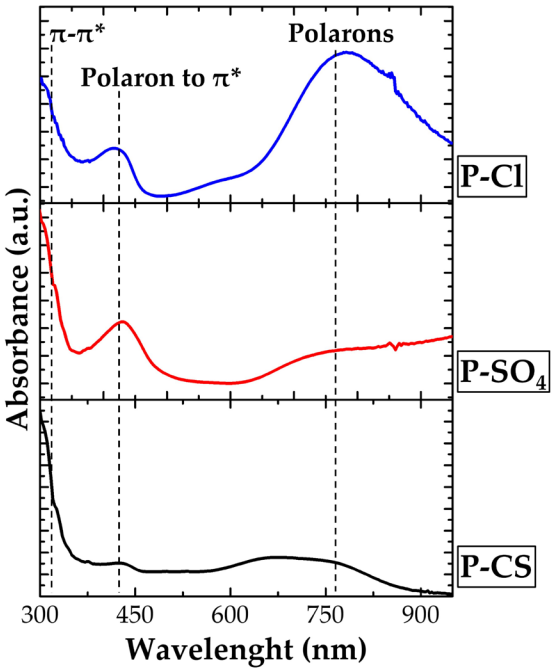

Figure 6. UV-vis spectra for P-Cl, P-SO_4, and P-CS samples along with main signals' attribution.

Given all these considerations, the results collected by coupling Raman, FTIR, EPR, and UV-Vis spectroscopic techniques provide a coherent picture of how dopant identity crucially governs the polaron population, chain conformation, and degree of electronic delocalization in the produced PDANI phases.

In order to evaluate how the structural and compositional features of the polymer chains influence the functional properties of the material, electrical conductivity measurements were carried out on PDANI pellets using the four-probe technique. Electrical conductivity (σ) values of 400 ± 50, 160 ± 20, and 100 ± 10 S/m were derived for P-Cl, P-SO_4, and P-CS samples, respectively. Taking into account the results obtained by the spectroscopic analyses, the significantly higher σ values of P-Cl can be attributed to the small ionic radius of the chloride dopant anion, which allows for more efficient packing and closer interchain interactions in the polymer matrix. In agreement with other works [8,62,69,70], smaller dopant agents facilitate tighter π–π stacking and improve charge delocalization along the conjugated backbone, thus enhancing conductivity. Moreover, the remarkable protonation degree (82%) observed from Raman analysis for P-Cl supports this outcome, as protonation is directly related to the formation of polarons.

In the case of P-SO_4, the measured electrical conductivity is about half that of P-Cl. Based on the spectroscopic analyses, this result can be explained by the combined effect of multiple factors. On one hand, the lower concentration of polarons in P-SO_4 limits the efficiency of charge transport [65–68]. On the other hand, the polymer chains in this sample appear to be more ordered at the molecular level, as supported by Raman spectroscopy [30,34,44]. This structural ordering may enhance interchain charge mobility, partially offsetting the reduced doping level and resulting in an intermediate conductivity, which is higher than P-CSA but lower than P-Cl. Ultimately, these observations emphasize

the critical role of the dopant. In agreement with other works [62–64], sulfuric acid not only acts as a dopant but can also behave as a templating agent, promoting enhanced chain alignment and crystallinity. This structural effect can partially compensate for a lower density of charge carriers, maintaining a respectable conductivity despite a limited polaron population.

Finally, the P-CS sample exhibits the lowest conductivity (100 S/m), despite a high protonation level (80%) and spectral features broadly similar to P-Cl in both FTIR and Raman analyses. On the basis of UV-Vis and EPR spectroscopies analyses, this discrepancy can be tentatively explained by the bulky nature of camphor sulfonate, which limits the doping efficiency and introduces steric hindrance that may disrupt chain packing [39]. As a result, the effective carrier mobility and interchain hopping probability are reduced, which is reflected in a conductivity roughly one-quarter of that of P-Cl.

Putting together all these findings, we can argue that not only the protonation level but also the size, structure, and chemical nature of the dopants critically influence the conductivity of PDANI. Small, compact dopants like Cl^- are more effective in promoting both doping efficiency and interchain interactions, while larger, more sterically hindered dopants like CS^- can limit charge transport even in well-protonated structures.

To investigate the electrochemical properties, the CV response of the produced P-Cl, P-SO_4, and P-CSA samples was tested in a 1 M HCl aqueous solution at 15, 30, 60, 120, and 200 mV/s (Figure 7). For each PDANI sample, CV measurements were always performed over multiple consecutive cycles, disclosing reproducible electrochemical stability of the synthesized PDANI powders.

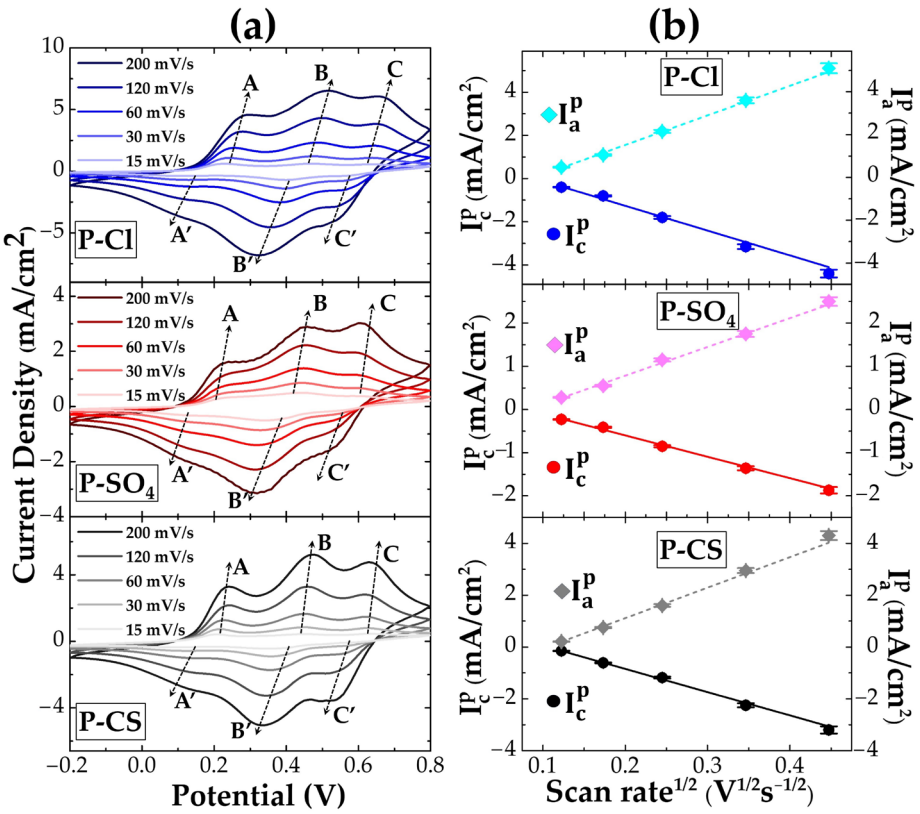

Figure 7. (**a**) CV curves at 15, 30, 60, 120, and 200 mV/s for P-Cl, P-SO_4, and P-CS samples in a 1 M HCl solution; (**b**) anodic and cathodic peak currents as a function of the scan rates' square root for P-Cl, P-SO_4, and P-CS samples.

As a direct consequence of the different electrical conductivities among the samples, the current densities in the CV curves of P-Cl are nearly twice as high as those measured

for P-SO_4 and P-CSA (Figure 7a). Despite these variations in absolute current densities, all three samples exhibit similar current–potential profiles, characterized by three pairs of quasi-reversible redox peaks (AA′, BB′, and CC′). These features are commonly attributed to stepwise redox transitions: AA′ corresponds to the leucoemeraldine-to-emeraldine (L–E) transformation, CC′ corresponds to the emeraldine-to-pernigraniline (E–P) transition, and BB′ is typically assigned to intermediate species, such as p-benzoquinone/hydroquinone, which arise during partial oxidation of the polymer backbone [2,25,44,77,78]. Additionally, the AA′ pair may also reflect hydrogen adsorption/desorption processes involving the polymer units [79,80].

A shift of both anodic and cathodic peaks with increasing scan rate is evident for the P-Cl, P-SO_4, and P-CS samples (black dashed arrows in Figure 7a), indicating a diffusion-controlled redox mechanism. This is further confirmed by the linear dependence of both anodic and cathodic peak currents on the square root of the scan rate (Figure 7b). The fit parameters are shown in Table 2.

Table 2. Linear regression equations and corresponding R^2 values for the anodic and cathodic peak currents as a function of the square root of the scan rate for P-Cl, P-SO_4, and P-CS samples.

Sample	Equation	R^2
P-Cl	I_c^p: y = −11.5x + 1.1	0.993
	I_a^p: y = 13.8x − 1.2	0.989
P-SO4	I_c^p: y = −5x + 0.4	0.995
	I_a^p: y = 6.7x − 0.5	0.994
P-CS	I_c^p: y = −7.6x + 0.8	0.986
	I_a^p: y = 10.3x − 1.1	0.991

As shown in Table 2, the linear correlation confirms that the redox processes proceed under diffusion-controlled conditions. Moreover, the ratio of anodic to cathodic peak currents slightly exceeds the unity across all scan rates, reinforcing the interpretation of quasi-reversible electron transfer processes involving the PDANI chains.

Further insights into the redox mechanisms can be drawn from ion exchange behavior. During electrochemical cycling, structural rearrangements associated with electron transfer are typically accompanied by ion insertion and expulsion to maintain charge neutrality. These processes may proceed via either anion or cation exchange, depending on the dopant size and nature. The corresponding reactions are represented by the following equilibrium reactions [30,35,39]:

- Anion exchange (typical for small dopants like Cl^- and $SO_4{}^{2-}$):

$$\mathrm{PDANI} + \mathrm{nA}^- + \mathrm{nH_2O} \rightleftharpoons \left(\mathrm{PDANI}^{(\mathrm{n}+)} : \left(\mathrm{A}^-\right)_\mathrm{n} : \mathrm{nH_2O}\right) + \mathrm{ne}^- \quad (3)$$

- Cation exchange (expected for bulky dopants like camphor sulfonate, CS^-):

$$\mathrm{PDANI} : \left(\mathrm{A}^-\right)_\mathrm{n} : \left(\mathrm{C}^+\right)_\mathrm{n} \rightleftharpoons \mathrm{PDANI}^{\mathrm{n}+} : \left(\mathrm{A}^-\right)_\mathrm{n} + \mathrm{ne}^- + \mathrm{n\,C}^+ \quad (4)$$

When small anionic dopants such as Cl^- and $SO_4{}^{2-}$ are used, the redox process is primarily governed by anion exchange (Equation (3)). This mechanism involves anion insertion upon oxidation, leading to swelling of the polymer, and anion expulsion upon reduction, resulting in shrinkage. In contrast, with bulky dopants like CS^-, the system is

more likely to undergo cation exchange (Equation (4)), with the reverse conformational changes occurring.

For each sample, the areal capacitance Ca ($mF \cdot cm^{-2}$) at 15 mV/s was calculated as reported in [35]. The Ca values of 40 ± 2, 12 ± 1, and 15 ± 1 $mF \cdot cm^{-2}$ were respectively derived for P-Cl, P-SO_4, and P-CS samples, corroborating how the dopant agent can drive the charge transport properties of the PDANI phases.

Among the samples studied, P-Cl exhibits the best electrochemical performance, as evidenced by both its high conductivity and the most intense areal capacitance and CV responses. This behavior reflects the efficient doping associated with the minimal steric hindrance of Cl^- ions, which promotes interchain interactions and a more effective charge transport mechanism.

Additional information on the charge transport properties can be achieved by QV analysis. Figure 8 illustrates the coulovoltammetric profiles for the three samples.

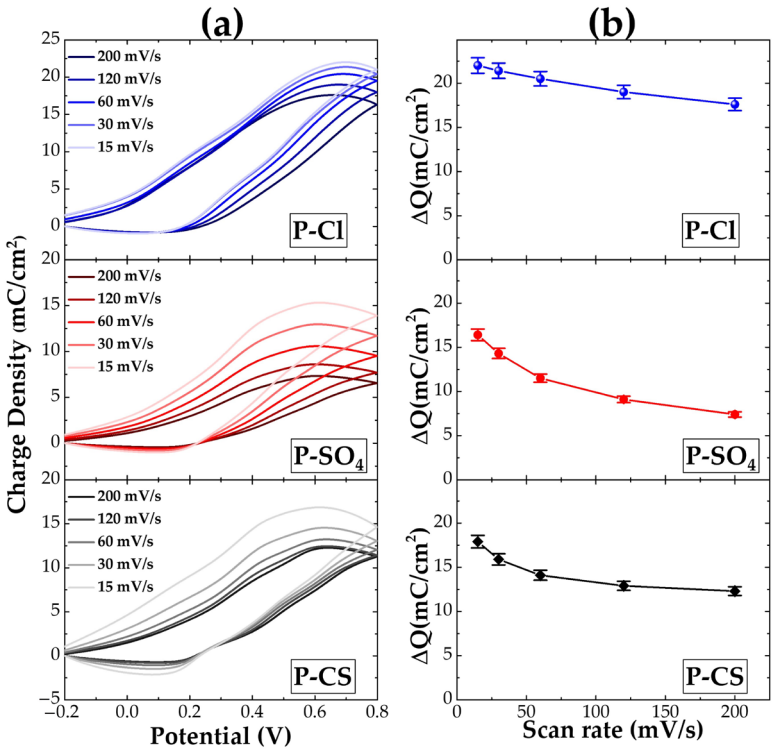

Figure 8. (**a**) Charge density (Q) vs. potential curves at scan rates of 15, 30, 60, 120, and 200 mV/s; (**b**) reversible charge (ΔQ), calculated as the difference between the maximum oxidation and reduction charges, as a function of the scan rate for P-Cl, P-SO_4, and P-CS samples.

As shown in Figure 8a, which displays the charge density (Q) as a function of potential at various scan rates (15–200 mV/s), all samples exhibit scan rate-dependent behavior. To better visualize such a dependence, Figure 8b reports the reversible charge (ΔQ), calculated as the difference between the maximum oxidation and reduction charges at each scan rate. As shown in Figure 8b, the general trend of ΔQ values is to decrease as a function of the scan rate for all the samples, corroborating the quasi-reversible redox behavior disclosed by CV analysis. However, the nature of the dopant agent induces rather different behaviors among the three samples. In particular, P-Cl exhibits the highest and most consistent ΔQ values across the scan rate range, which can be attributed to the small ionic radius and monovalent nature of Cl^- ions. These properties enable rapid and efficient anion insertion and expulsion during redox cycling, minimizing steric hindrance and promoting uniform charge distribution and compensation along the polymer chains. This leads to enhanced ionic mobility and improved coupling between electron and ion transport,

resulting in superior electrochemical performance under both low and high scan rate conditions [8,62,69,70]. Conversely, although showing a relatively high ΔQ at low scan rates, P-SO_4 suffers from a steep decline as the scan rate increases. This behavior can be tentatively ascribed to the bivalency of SO_4^{2-} and to the larger size with respect to Cl^- ions. The synergic contribution of such properties probably hinders rapid diffusion and reduces electrochemical efficiency under dynamic conditions. On the other hand, P-CS shows a more stable profile across increasing scan rates compared to P-SO_4. This suggests that the redox processes in P-CS are less diffusion-limited. A plausible explanation lies in the different ion exchange mechanism: unlike Cl^- and SO_4^{2-}, which undergo anion exchange, CS^- is bulky and likely promotes a cation-exchange mechanism, reasonably involving H^+ insertion/expulsion. The high concentration of available protons may enhance ionic mobility and reduce kinetic barriers, resulting in better retention of charge at high scan rates. These findings emphasize the importance of dopant identity not only in determining redox capacity but also in governing the charge transport mechanisms, especially under non-equilibrium regimes.

Based on the QV analysis, we can draw important conclusions regarding the possible use of PDANI-based systems in electrochemical applications. P-Cl emerges as the most promising candidate for high-performance supercapacitors, thanks to its high and stable reversible charge even at fast scan rates [39,57,63,64]. This indicates excellent redox reversibility, efficient charge transport, and low ion diffusion limitations, which are key features for devices requiring fast charge/discharge cycles and high-power density. A different use can be designed for P-CS systems. Despite having a ΔQ lower than the P-Cl sample, P-CS shows greater stability across scan rates, likely due to a cation exchange mechanism facilitated by proton mobility. This makes P-CS suitable for battery-type systems, where slower but more controlled charge processes and longer cycling life are beneficial [29,81]. Finally, the behavior of P-SO_4 polymer, characterized by higher ΔQ at low scan rates but pronounced decay at higher rates, may be less ideal for high-rate applications [82,83]. However, it could be useful in hybrid energy storage systems, where energy density is favored over power density, provided operating conditions are optimized.

Taken together, the results of the structural, electrochemical, and electrical characterizations clearly demonstrate that the nature of the dopant plays a central role in governing the chemical, physical, and functional properties of the final PDANI polymer. From molecular organization and oxidation/protonation levels to charge transport efficiency and redox performance, each dopant distinctly influences the behavior of the final material. These findings underscore the importance of dopant selection as a key parameter in tailoring PDANI for specific applications, particularly in the field of energy storage and electrochemical devices.

4. Conclusions

In this work, polydianiline (PDANI) polymer systems were successfully synthesized starting from dianiline, a sustainable and low-toxicity monomer precursor. The synthesis was carried out under mild, green conditions using aqueous and DMSO-based media, with the resulting materials obtained in the emeraldine salt form.

A comprehensive multi-technique characterization approach was employed to evaluate the relationships occurring between the structural and electrochemical features of the PDANI samples. Specifically, spectroscopic techniques (FTIR, Raman, EPR, UV-Vis) provided insights into the molecular structure, chemical composition, and polaron population, while electrochemical methods (I-V, CV, QV) enabled us to assess the conductivity, redox activity, and charge storage capacity.

In view of the results obtained, the study clearly demonstrates that the nature of the dopant and the acidic medium used during synthesis plays a crucial role in tailoring the final properties of PDANI. The chloride-doped PDANI sample showed the highest polaron population and conductivity, making it suitable for high-power applications. The sulfate-doped PDANI sample exhibited higher molecular ordering but a lower charge carrier density. Finally, despite its steric hindrance, camphor sulfonate-doped PDANI led to a material with moderate conductivity and stable electrochemical performance.

This work provides valuable insight into how synthetic parameters influence PDANI properties and opens up new possibilities for its use in printed electronics, energy storage systems, and green polymer-based devices.

Author Contributions: Conceptualization, S.B. and R.C.; methodology, S.B. and R.C.; software, R.C., G.S.; validation, S.B. and E.T.; formal analysis, R.C.; investigation (experimental work), R.C., F.P., L.M., E.P. and S.B.; resources, S.B., E.T. and A.C.; data curation, R.C. and S.B.; writing—original draft preparation, R.C.; writing—review and editing, S.B. and E.T.; visualization, S.B. and E.T.; supervision, S.B. and E.T.; project administration, S.B.; funding acquisition, S.B. All authors have read and agreed to the published version of the manuscript.

Funding: This research was funded by the CNR project: "Hardware realization of reservoir computing and pattern recognition systems based on deterministic and stochastic organic memristive devices," grant number B55F20002250005.

Data Availability Statement: The data supporting the findings of this study are available from the corresponding author upon reasonable request. All relevant experimental details, characterization data, and analysis are included in the manuscript.

Acknowledgments: R.C. acknowledges Adriano Verna for the support in EPR measurements. E.T. acknowledges the MUR Grant "Departments of Excellence 2023–2027" under the X-CHEM project "eXpanding CHEMistry: implementing excellence in research and teaching" awarded to the Department of Chemical Science and Technologies, University of Rome Tor Vergata. GenAI has been used in this paper to edit and adjust the text.

Conflicts of Interest: The authors declare no conflicts of interest.

References

1. Shirakawa, H.; Louis, E.J.; MacDiarmid, A.G.; Chiang, C.K.; Heeger, A.J. Synthesis of Electrically Conducting Organic Polymers: Halogen Derivatives of Polyacetylene, (CH) X. *J. Chem. Soc. Chem. Commun.* **1977**, *16*, 578–580. [CrossRef]
2. Popov, A.; Brasiunas, B.; Mikoliunaite, L.; Bagdziunas, G.; Ramanavicius, A.; Ramanaviciene, A. Comparative Study of Polyaniline (PANI), Poly(3,4-Ethylenedioxythiophene) (PEDOT) and PANI-PEDOT Films Electrochemically Deposited on Transparent Indium Thin Oxide Based Electrodes. *Polymer* **2019**, *172*, 133–141. [CrossRef]
3. Kumar, V.; Mirzaei, A.; Bonyani, M.; Kim, K.H.; Kim, H.W.; Kim, S.S. Advances in Electrospun Nanofiber Fabrication for Polyaniline (PANI)-Based Chemoresistive Sensors for Gaseous Ammonia. *TrAC Trends Anal. Chem.* **2020**, *129*, 115938. [CrossRef]
4. Mazzara, F.; Patella, B.; D'agostino, C.; Bruno, M.G.; Carbone, S.; Lopresti, F.; Aiello, G.; Torino, C.; Vilasi, A.; O'riordan, A.; et al. Pani-Based Wearable Electrochemical Sensor for Ph Sweat Monitoring. *Chemosensors* **2021**, *9*, 169. [CrossRef]
5. Politi, S.; Carcione, R.; Tamburri, E.; Matassa, R.; Lavecchia, T.; Angjellari, M.; Terranova, M.L. Graphene Platelets from Shungite Rock Modulate Electropolymerization and Charge Storage Mechanisms of Soft-Template Synthetized Polypyrrole-Based Nanocomposites. *Sci. Rep.* **2018**, *8*, 17045. [CrossRef] [PubMed]
6. Zhao, Y.H.; Niu, C.M.; Shi, J.Q.; Wang, Y.Y.; Yang, Y.M.; Wang, H.B. Novel Conductive Polypyrrole/Silk Fibroin Scaffold for Neural Tissue Repair. *Neural Regen. Res.* **2018**, *13*, 1455. [CrossRef]
7. Yan, Y.; Jiang, Y.; Ng, E.L.L.; Zhang, Y.; Owh, C.; Wang, F.; Song, Q.; Feng, T.; Zhang, B.; Li, P.; et al. Progress and Opportunities in Additive Manufacturing of Electrically Conductive Polymer Composites. *Mater. Today Adv.* **2023**, *17*, 100333. [CrossRef]
8. Liao, G.; Li, Q.; Xu, Z. The Chemical Modification of Polyaniline with Enhanced Properties: A Review. *Prog. Org. Coat.* **2019**, *126*, 35–43. [CrossRef]
9. Carcione, R.; Marasso, S.L.; Guglielmotti, V.; Cocuzza, M.; Tamburri, E.; Battistoni, S. One-Pot and Mask-Less Realization Approach for Polypyrrole-Polydopamine-Based Organic Electrochemical Transistors. *ACS Appl. Electron. Mater.* **2025**, *7*, 2619–2628. [CrossRef]

10. Scordo, G.; Bertana, V.; Ballesio, A.; Carcione, R.; Marasso, S.L.; Cocuzza, M.; Pirri, C.F.; Manachino, M.; Gomez, M.G.; Vitale, A.; et al. Effect of Volatile Organic Compounds Adsorption on 3D-Printed Pegda:Pedot for Long-Term Monitoring Devices. *Nanomaterials* **2021**, *11*, 94. [CrossRef]
11. Cavallo, A.; Losi, P.; Buscemi, M.; Kayal, T.A.; Beccatelli, M.; Soldani, G.; Coppedè, N. Biocompatible Organic Electrochemical Transistor on Polymeric Scaffold for Wound Healing Monitoring. *Flex. Print. Electron.* **2022**, *7*, 035009. [CrossRef]
12. Colucci, R.; Feitosa, B.A.; Faria, G.C. Impact of Ionic Species on the Performance of Pedot:PSS-Based Organic Electrochemical Transistors. *Adv. Electron. Mater.* **2024**, *10*, 2300235. [CrossRef]
13. Battistoni, S.; Erokhin, V.; Iannotta, S. Frequency Driven Organic Memristive Devices for Neuromorphic Short Term and Long Term Plasticity. *Org. Electron.* **2019**, *65*, 434–438. [CrossRef]
14. Doan, T.C.D.; Ramaneti, R.; Baggerman, J.; Van Der Bent, J.F.; Marcelis, A.T.M.; Tong, H.D.; Van Rijn, C.J.M. Carbon Dioxide Sensing with Sulfonated Polyaniline. *Sens. Actuators B Chem.* **2012**, *168*, 123–130. [CrossRef]
15. Passeri, D.; Tamburri, E.; Terranova, M.L.; Rossi, M. Polyaniline–Nanodiamond Fibers Resulting from the Self-Assembly of Nano-Fibrils: A Nanomechanical Study. *Nanoscale* **2015**, *7*, 14358–14367. [CrossRef] [PubMed]
16. Medi, B.; Bahramian, A.; Nazari, V. Synthesis and Characterization of Conducting Polyaniline Nanostructured Thin Films for Solar Cell Applications. *JOM* **2021**, *73*, 504–514. [CrossRef]
17. Kamarudin, S.; Rani, M.S.A.; Mohammad, M.; Mohammed, N.H.; Su'ait, M.S.; Ibrahim, M.A.; Asim, N.; Razali, H. Investigation on Size and Conductivity of Polyaniline Nanofiber Synthesised by Surfactant-Free Polymerization. *J. Mater. Res. Technol.* **2021**, *14*, 255–261. [CrossRef]
18. Wei, X.; Epstein, A.J. Synthesis of Highly Sulfonated Polyaniline. *Synth. Met.* **1995**, *74*, 123–125. [CrossRef]
19. Chiolerio, A.; Bocchini, S.; Scaravaggi, F.; Porro, S.; Perrone, D.; Beretta, D.; Caironi, M.; Fabrizio Pirri, C. Synthesis of Polyaniline-Based Inks for Inkjet Printed Devices: Electrical Characterization Highlighting the Effect of Primary and Secondary Doping. *Semicond. Sci. Technol.* **2015**, *30*, 104001. [CrossRef]
20. Pyarasani, R.D.; Jayaramudu, T.; John, A. Polyaniline-Based Conducting Hydrogels. *J. Mater. Sci.* **2018**, *54*, 974–996. [CrossRef]
21. Yasuda, A.; Shimidzu, T. Chemical and Electrochemical Analyses of Polyaniline Prepared with $FeCl_3$. *Synth. Met.* **1993**, *61*, 239–245. [CrossRef]
22. Suendo, V.; Lau, Y.; Hidayat, F.; Reza, M.; Qadafi, A.; Rochliadi, A. Effect of Face-to-Face and Side-to-Side Interchain Interactions on the Electron Transport in Emeraldine Salt Polyaniline. *Phys. Chem. Chem. Phys.* **2021**, *23*, 7190–7199. [CrossRef]
23. Banjar, M.F.; Joynal Abedin, F.N.; Fizal, A.N.S.; Muhamad Sarih, N.; Hossain, M.S.; Osman, H.; Khalil, N.A.; Ahmad Yahaya, A.N.; Zulkifli, M. Synthesis and Characterization of a Novel Nanosized Polyaniline. *Polymers* **2023**, *15*, 4565. [CrossRef]
24. Xia, Y.; Wiesinger, J.M.; MacDiarmid, A.G.; Epstein, A.J. Camphorsulfonic acid fully doped polyaniline emeraldine salt: Conformations in different solvents studied by an ultraviolet/visible/near-infrared spectroscopic method. *Chem. Mater.* **1995**, *7*, 433–445. [CrossRef]
25. Jamadade, V.S.; Dhawale, D.S.; Lokhande, C.D. Studies on Electrosynthesized Leucoemeraldine, Emeraldine and Pernigraniline Forms of Polyaniline Films and Their Supercapacitive Behavior. *Synth. Met.* **2010**, *160*, 955–960. [CrossRef]
26. Sanches, E.A.; Soares, J.C.; Iost, R.M.; Marangoni, V.S.; Trovati, G.; Batista, T.; Mafud, A.C.; Zucolotto, V.; Mascarenhas, Y.P. Structural Characterization of Emeraldine-Salt Polyaniline/Gold Nanoparticles Complexes. *J. Nanomater.* **2011**, *2011*, 697071. [CrossRef]
27. Junker, K.; Luginbühl, S.; Schüttel, M.; Bertschi, L.; Kissner, R.; Schuler, L.D.; Rakvin, B.; Walde, P. Efficient Polymerization of the Aniline Dimer p -Aminodiphenylamine (PADPA) with Trametes Versicolor Laccase/O2 as Catalyst and Oxidant and AOT Vesicles as Templates. *ACS Catal.* **2014**, *4*, 3421–3434. [CrossRef]
28. Mir, A.; Kumar, A.; Riaz, U. A Short Review on the Synthesis and Advance Applications of Polyaniline Hydrogels. *RSC Adv.* **2022**, *12*, 19122–19132. [CrossRef] [PubMed]
29. Goswami, S.; Nandy, S.; Fortunato, E.; Martins, R. Polyaniline and Its Composites Engineering: A Class of Multifunctional Smart Energy Materials. *J. Solid State Chem.* **2023**, *317*, 123679. [CrossRef]
30. Montaina, L.; Carcione, R.; Pescosolido, F.; Montalto, M.; Battistoni, S.; Tamburri, E. Three-Dimensional-Printed Polyethylene Glycol Diacrylate-Polyaniline Composites by in Situ Aniline Photopolymerization: An Innovative Biomaterial for Electrocardiogram Monitoring Systems. *ACS Appl. Electron. Mater.* **2022**, *5*, 164–172. [CrossRef]
31. Demin, V.A.; Erokhin, V.V.; Emelyanov, A.V.; Battistoni, S.; Baldi, G.; Iannotta, S.; Kashkarov, P.K.; Kovalchuk, M.V. Hardware Elementary Perceptron Based on Polyaniline Memristive Devices. *Org. Electron.* **2015**, *25*, 16–20. [CrossRef]
32. Li, H.; Zhou, J.; Lu, X.; Wang, J.; Qu, S.; Weng, J.; Feng, B. Camphorsulfonic Acid-Doped Polyaniline/TiO_2 Nanotube Hybrids: Synthesis Strategy and Enhanced Visible Photocatalytic Activity. *J. Mater. Sci. Mater. Electron.* **2015**, *26*, 7723–7730. [CrossRef]
33. Poddar, A.K.; Patel, S.S.; Patel, H.D. Synthesis, Characterization and Applications of Conductive Polymers: A Brief Review. *Polym. Adv. Technol.* **2021**, *32*, 4616–4641. [CrossRef]
34. Carcione, R.; Pescosolido, F.; Montaina, L.; Toschi, F.; Orlanducci, S.; Tamburri, E.; Battistoni, S. Self-Standing 3D-Printed PEGDA–PANIs Electroconductive Hydrogel Composites for PH Monitoring. *Gels* **2023**, *9*, 784. [CrossRef]

35. Politi, S.; Battistoni, S.; Carcione, R.; Montaina, L.; Macis, S.; Lupi, S.; Tamburri, E. PANI-Modified Ti-Doped CVD Diamond As Promising Conductive Platform to Mimic Bioelectricity Functions. *Adv. Mater. Interfaces* **2021**, *8*, 2101401. [CrossRef]
36. Korent, A.; Žagar Soderžnik, K.; Šturm, S.; Žužek Rožman, K. A Correlative Study of Polyaniline Electropolymerization and Its Electrochromic Behavior. *J. Electrochem. Soc.* **2020**, *167*, 106504. [CrossRef]
37. Giacobbe, S.; Pezzella, C.; Della Ventura, B.; Giacobelli, V.G.; Rossi, M.; Fontanarosa, C.; Amoresano, A.; Sannia, G.; Velotta, R.; Piscitelli, A. Green Synthesis of Conductive Polyaniline by Trametes Versicolor Laccase Using a DNA Template. *Eng. Life Sci.* **2019**, *19*, 631–642. [CrossRef]
38. Ranjith Kumar, D.; Dhakal, G.; Muhammed Shafi, P.; Saad Sayed, M.; Lee, J.; Lee, Y.R.; Shim, J.J. Sulfite Food Additive Electrochemical Determination by Nucleophilic Addition on Poly(4-Aminodiphenylamine)-4-Aminothiophenol-Au Composite Electrode. *Microchem. J.* **2022**, *181*, 107635. [CrossRef]
39. Carcione, R.; Roppolo, I.; Chiappone, A.; Cocuzza, M.; Marasso, S.L.; Tamburri, E.; Battistoni, S. Role of Precursors and Doping Agents in Producing 3D-Printed PEGDA-PDANI Electroactive Composites by an In Situ Polymerization Approach. *ACS Appl. Polym. Mater.* **2024**, *6*, 1159–1168. [CrossRef]
40. Li, X.G.; Huang, M.R.; Duan, W.; Yang, Y.L. Novel Multifunctional Polymers from Aromatic Diamines by Oxidative Polymerizations. *Chem. Rev.* **2002**, *102*, 2925–3030. [CrossRef]
41. Zhao, R.; Peng, H.; Wang, F.; Zhen, J.; Li, L.; Ma, G.; Lei, Z. Regulating the Species and the Counter-Ion Size of Proton Acids to Prepare Novel Poly(4-Aminodiphenylamine) Nanomaterials for Supercapacitors. *Mater. Chem. Front.* **2021**, *5*, 6145–6151. [CrossRef]
42. Lin, C.W.; Mak, W.H.; Chen, D.; Wang, H.; Aguilar, S.; Kaner, R.B. Catalytic Effects of Aniline Polymerization Assisted by Oligomers. *ACS Catal.* **2019**, *9*, 6596–6606. [CrossRef]
43. Peng, H.; Zhao, R.; Liang, J.; Wang, S.; Wang, F.; Zhou, J.; Ma, G.; Lei, Z. Template-Confined Growth of Poly(4-Aminodiphenylamine) Nanosheets as Positive Electrode toward Superlong-Life Asymmetric Supercapacitor. *ACS Appl. Mater. Interfaces* **2018**, *10*, 37125–37134. [CrossRef]
44. Pescosolido, F.; Montaina, L.; Carcione, R.; Politi, S.; Matassa, R.; Carotenuto, F.; Nottola, S.A.; Nardo, P.D.; Tamburri, E. A New Strong-Acid Free Route to Produce Xanthan Gum-PANI Composite Scaffold Supporting Bioelectricity. *Macromol. Biosci.* **2023**, *23*, 2300132. [CrossRef]
45. Politi, S.; Tamburri, E.; Carcione, R.; Lavecchia, T.; Angjellari, M.; Terranova, M.L. Innovative Preparation Processes and Structural Characteristics of 3D Printable Polymer-Based Nanocomposites. In Proceedings of the AIP Conference Proceedings, Lakeland, FL, USA, 17–19 January 2019; Volume 2196.
46. Galloni, M.G.; Della Pina, C.; Bortolotto, V.; Nikonova, V.; Falletta, E.; Bianchi, C.L. Highly Porous Polyaniline (PANI): A Novel Green Catalytic Method for Morphology Control. *J. Mater. Sci.* **2025**, *60*, 5300–5325. [CrossRef]
47. Zhu, D.; Cheng, K.; Wang, Y.; Sun, D.; Gan, L.; Chen, T.; Jiang, J.; Liu, M. Nitrogen-Doped Porous Carbons with Nanofiber-like Structure Derived from Poly (Aniline-Co-p-Phenylenediamine) for Supercapacitors. *Electrochim. Acta* **2017**, *224*, 17–24. [CrossRef]
48. Levi, M.D.; Lapkowski, M. Mechanism of Electron Transfer during the Course of Oxidation of N-Phenyl-p-Phenylenediamine Polythiophene and Poly-3-Methylthiophene Coated Electrodes: Redox Catalysis versus Outer-Sphere Heterogeneous Electron Transfer. *Electrochim. Acta* **1993**, *38*, 271–279. [CrossRef]
49. Wang, Y.Z.; Ko, T.H.; Huang, W.Y.; Hsieh, T.H.; Ho, K.S.; Chen, Y.Y.; Hsieh, S.J. Preparation of Pt-Catalyst by Poly(p-Phenylenediamine) Nanocomposites Assisted by Microwave Radiation for Proton Exchange Membrane Fuel Cell. *Polymers* **2018**, *10*, 1388. [CrossRef]
50. Tsai, M.J.; Hsieh, T.H.; Wang, Y.Z.; Ho, K.S.; Chang, C.Y. Microwave Assisted Reduction of Pt-Catalyst by N-Phenyl-p-Phenylenediamine for Proton Exchange Membrane Fuel Cells. *Polymers* **2017**, *9*, 104. [CrossRef]
51. Yao, C.J.; Xie, J.; Wu, Z.; Xu, Z.J.; Zhang, S.; Zhang, Q. A Conjugated Copolymer of N-Phenyl-p-Phenylenediamine and Pyrene as Promising Cathode for Rechargeable Lithium–Ion Batteries. *Chem. Asian J.* **2019**, *14*, 2210–2214. [CrossRef]
52. Stejskal, J.; Trchová, M.; Bober, P.; Humpolíček, P.; Kašpárková, V.; Sapurina, I.; Shishov, M.A.; Varga, M. Conducting Polymers: Polyaniline. *Encycl. Polym. Sci. Technol.* **2015**, *35*, 1–44. [CrossRef]
53. Yuan, J.; Hu, X.; Zhao, X.; Yin, J. Electrorheological Effect of Suspensions of Polyaniline Nanoparticles with Different Morphologies. *Polymers* **2023**, *15*, 4568. [CrossRef]
54. Su, N. Polyaniline-Doped Spherical Polyelectrolyte Brush Nanocomposites with Enhanced Electrical Conductivity, Thermal Stability, and Solubility Property. *Polymers* **2015**, *7*, 1599–1616. [CrossRef]
55. Shao, W.; Jamal, R.; Xu, F.; Ubul, A.; Abdiryim, T. The Effect of a Small Amount of Water on the Structure and Electrochemical Properties of Solid-State Synthesized Polyaniline. *Materials* **2012**, *5*, 1811–1825. [CrossRef]
56. Prabhu, R.; Jeevananda, T.; Reddy, K.R.; Raghu, A.V. Polyaniline-Fly Ash Nanocomposites Synthesized via Emulsion Polymerization: Physicochemical, Thermal and Dielectric Properties. *Mater. Sci. Energy Technol.* **2021**, *4*, 107–112. [CrossRef]

57. Aziz, D.M.; Hassan, S.A.; Aziz, S.B. Synthesis and Characterization of Enhanced Azo-Azomethine Doped PANI/HCl Conducting Polymers for Electrochemical Applications. *Sci. Rep.* **2024**, *14*, 18122. [CrossRef]
58. Wang, J.; Wang, J.; Yang, Z.; Wang, Z.; Zhang, F.; Wang, S. A Novel Strategy for the Synthesis of Polyaniline Nanostructures with Controlled Morphology. *React. Funct. Polym.* **2008**, *68*, 1435–1440. [CrossRef]
59. Tamburri, E.; Guglielmotti, V.; Orlanducci, S.; Terranova, M.L.; Sordi, D.; Passeri, D.; Matassa, R.; Rossi, M. Nanodiamond-Mediated Crystallization in Fibers of PANI Nanocomposites Produced by Template-Free Polymerization: Conductive and Thermal Properties of the Fibrillar Networks. *Polymer* **2012**, *53*, 4045–4053. [CrossRef]
60. Lindfors, T.; Ivaska, A. Raman Based PH Measurements with Polyaniline. *J. Electroanal. Chem.* **2005**, *580*, 320–329. [CrossRef]
61. Shakoor, A.; Rizvi, T.Z.; Nawaz, A. Raman Spectroscopy and AC Conductivity of Polyaniline Montmorillonite (PANI-MMT) Nanocomposites. *J. Mater. Sci. Mater. Electron.* **2011**, *22*, 1076–1080. [CrossRef]
62. Bednarczyk, K.; Matysiak, W.; Tański, T.; Janeczek, H.; Schab-Balcerzak, E.; Libera, M. Effect of Polyaniline Content and Protonating Dopants on Electroconductive Composites. *Sci. Rep.* **2021**, *11*, 7487. [CrossRef]
63. Zhou, S.X.; Tao, X.Y.; Ma, J.; Qu, C.H.; Zhou, Y.; Guo, L.T.; Feng, P.Z.; Zhu, Y.B.; Wei, X.Y. Facile Synthesis of Self-Assembled Polyaniline Nanorods Doped with Sulphuric Acid for High-Performance Supercapacitors. *Vacuum* **2017**, *143*, 63–70. [CrossRef]
64. Shen, Y.; Qin, Z.; Li, T.; Zeng, F.; Chen, Y.; Liu, N. Boosting the Supercapacitor Performance of Polyaniline Nanofibers through Sulfonic Acid Assisted Oligomer Assembly during Seeding Polymerization Process. *Electrochim. Acta* **2020**, *356*, 136841. [CrossRef]
65. Krinichnyi, V.I.; Roth, H.K.; Schrödner, M.; Wessling, B. EPR Study of Polyaniline Highly Doped by P-Toluenesulfonic Acid. *Polymer* **2006**, *47*, 7460–7468. [CrossRef]
66. Gupta, S.K.; Luthra, V.; Singh, R. Electrical Transport and EPR Investigations: A Comparative Study for d.c. Conduction Mechanism in Monovalent and Multivalent Ions Doped Polyaniline. *Bull. Mater. Sci.* **2012**, *35*, 787–794. [CrossRef]
67. Krinichnyi, V.; Chemerisov, S.; Lebedev, Y.S. EPR and Charge-Transport Studies of Polyaniline. *Phys. Rev. B* **1997**, *55*, 16233. [CrossRef]
68. Krinichnyi, V.I.; Roth, H.K.; Hinrichsen, G.; Lux, F.; Lüders, K. EPR and Charge Transfer in H_2SO_4-Doped Polyaniline. *Phys. Rev. B* **2002**, *65*, 155205. [CrossRef]
69. Zhang, Z.; Wei, Z.; Wan, M. Nanostructures of Polyaniline Doped with Inorganic Acids. *Macromolecules* **2002**, *35*, 5937–5942. [CrossRef]
70. Sinha, S.; Bhadra, S.; Khastgir, D. Effect of Dopant Type on the Properties of Polyaniline. *J. Appl. Polym. Sci.* **2009**, *112*, 3135–3140. [CrossRef]
71. Arora, M.; Luthra, V.; Singh, R.; Gupta, S.K. Vibrational Spectra of Acid-Doped Polyaniline Study of Vibrational Spectra of Polyaniline Doped with Sulfuric Acid and Phosphoric Acid. *Appl. Biochem. Biotechnol.* **2001**, *96*, 173–181. [CrossRef]
72. Nunes, W.G.; Pires, B.M.; Thaines, E.H.N.S.; Pereira, G.M.A.; da Silva, L.M.; Freitas, R.G.; Zanin, H. Operando Raman Spectroelectrochemical Study of Polyaniline Degradation: A Joint Experimental and Theoretical Analysis. *J. Energy Storage* **2022**, *55*, 105770. [CrossRef]
73. Udayaraj, S.; Annappa, M.; Roopa, K.V.; Mathad, G.; Subramanya, K.; Pavithra, G.M. Optical, Structural and Conductivity Properties of Ferrous Sulfate Doped Polyaniline. *Mater. Today Proc.* **2024**, *100*, 132–138. [CrossRef]
74. Ting, C.-Y.; Wu, P.-L.; Huang, C.-C.; Andreas, R.; Lesbani, A.; Yusuf, F.A. The Character Istics (Compositions, Morphological, and Structure) of Nanocomposites Polyaniline (PANI)/ZnO. *IOP Conf. Ser. Mater. Sci. Eng.* **2019**, *509*, 012126. [CrossRef]
75. Moulton, S.E.; Innis, P.C.; Kane-Maguire, L.A.P.; Ngamna, O.; Wallace, G.G. Polymerisation and Characterisation of Conducting Polyaniline Nanoparticle Dispersions. *Curr. Appl. Phys.* **2004**, *4*, 402–406. [CrossRef]
76. Wong, P.Y.; Phang, S.W.; Baharum, A. Effects of Synthesised Polyaniline (PAni) Contents on the Anti-Static Properties of PAni-Based Polylactic Acid (PLA) Films. *RSC Adv.* **2020**, *10*, 39693–39699. [CrossRef] [PubMed]
77. Chen, W.C.; Wen, T.C.; Hu, C.C.; Gopalan, A. Identification of Inductive Behavior for Polyaniline via Electrochemical Impedance Spectroscopy. *Electrochim. Acta* **2002**, *47*, 1305–1315. [CrossRef]
78. Kuzmany, H.; Sariciftci, N.S. In Situ Spectro-Electrochemical Studies of Polyaniline. *Synth. Met.* **1987**, *18*, 353–358. [CrossRef]
79. Biabangard, F.; Nazari, H.; Arefinia, R. Effect of PH on the Electrochemical Properties of Polyaniline Nanoparticle Suspension in Strongly Acidic Solution: An Experimental and Theoretical Study. *J. Solid State Electrochem.* **2021**, *25*, 881–893. [CrossRef]
80. Yan, B.; Yang, J.; Li, Y.; Cao, Y. Electrochemical Adsorption of Hydrogen and Various Ions on Polyaniline Film. Reactions Concerning the First Pair of Cyclic Voltammetric Peaks. *Synth. Met.* **1991**, *44*, 189–197. [CrossRef]
81. Garrudo, F.F.F.; Ferreira, L.F.V.; Ferraria, A.M.; do Rego, A.M.B.; Charas, A.; André, V.; Duarte, M.T.; Linhardt, R.J.; Ferreira, F.C.; Morgado, J. Pseudo-Doping Effect on Structural and Electrical Properties of Polyaniline-Camphorsulfonic Acid. *Synth. Met.* **2024**, *301*, 117523. [CrossRef]

82. Luo, Y.; Guo, R.; Li, T.; Li, F.; Liu, Z.; Zheng, M.; Wang, B.; Yang, Z.; Luo, H.; Wan, Y. Application of Polyaniline for Li-Ion Batteries, Lithium–Sulfur Batteries, and Supercapacitors. *ChemSusChem* **2019**, *12*, 1591–1611. [CrossRef] [PubMed]
83. Ryu, K.S.; Jeong, S.K.; Joo, J.; Kim, K.M. Polyaniline Doped with Dimethyl Sulfate as a Nucleophilic Dopant and Its Electrochemical Properties as an Electrode in a Lithium Secondary Battery and a Redox Supercapacitor. *J. Phys. Chem. B* **2007**, *111*, 731–739. [CrossRef] [PubMed]